Neurobiology of Pain 13 (2023) 100116

Contents lists available at ScienceDirect

Neurobiology of Pain

journal homepage: www.sciencedirect.com/journal/neurobiology-of-pain

Betulinic acid analogs inhibit N- and T-type voltage-gated calcium channels to attenuate nerve-injury associated neuropathic and formalin models of pain

Aida Calderon-Rivera [a,b], Kimberly Gomez [a,b], Santiago Loya-López [a,b], E.M. Kithsiri Wijeratne [c], Harrison Stratton [d], Cheng Tang [a,b], Paz Duran [a,b], Kyleigh Masterson [b], Omar Alsbiei [b], A.A. Leslie Gunatilaka [c], Rajesh Khanna [a,b,*,1]

[a] Department of Molecular Pathobiology, College of Dentistry, New York University, New York, NY, United States
[b] NYU Pain Research Center, New York University, New York, NY, United States
[c] Natural Products Center, School of Natural Resources and the Environment, College of Agriculture and Life Sciences, The University of Arizona, Tucson, AZ, United States
[d] Department of Pharmacology, College of Medicine, The University of Arizona, Tucson, AZ, United States

ARTICLE INFO

Keywords:
Betulinic acid analogs
Betulin analogs
Voltage-gated calcium channels
Analgesic
Spared nerve injury mode
Formalin model
Pain

ABSTRACT

Over the past three decades, there has been a significant growth in the use of natural products, with approximately 80% of individuals using them for some aspect of primary healthcare. Our laboratories have identified and studied natural compounds with analgesic effects from dry land plants or their associated fungus during the past ten years. Here, we isolated and characterized thirteen betulin analogs and fifteen betulinic acid analogs for their capacity to prevent calcium influx brought on by depolarization in sensory neurons. The in vitro inhibition of voltage-gated calcium channels by the top drugs was then assessed using whole cell patch clamp electrophysiology. In vivo experiments, conducted at two sites, evaluated the best compound in acute and tonic, neuropathic, inflammatory, post-operative and visceral models of pain. We found that the betulinic acid analog **8** inhibited calcium influx in rat dorsal root ganglion neurons by inhibiting N- (CaV2.2) and T- (CaV3) type voltage-gated calcium channels. Moreover, intrathecal delivery of analog **8** had analgesic activity in both spared nerve injury model of neuropathic pain and acute and tonic pain induced by formalin. The results presented herein highlight the potential antinociceptive properties of betulinic acid analog **8** and set the stage for the development of novel non-opioid pain therapeutics based on the triterpenoid scaffold of betulinic acid.

Introduction

Data from the 2019 National Health Interview Survey highlighted that 20.4 % of adults had chronic pain and 7.4 % suffered from high impact chronic pain that frequently limited life or work activities (Zelaya et al., 2019). Chronic pain likely results from persistent hyperactivity of specialized sensory neurons called nociceptors (Walters et al., 2022). Amplification of primary afferent signaling contributing to chronic pain can result from distinct processes including dysregulation of proteins involved in transduction, transmission, and processing of sensory information (Tibbs et al., 2016). In particular, the expression and function of ion channels adapt from a physiologically hypervigilant function to one contributing to a pathological pain state. Such changes can lead to increase in both spontaneous activity and increased responsivity to sensory stimuli (Walters et al., 2022; Tibbs et al., 2016; Vicario et al., 2020).

Voltage-gated calcium channels (VGCCs) are expressed in the central and peripheral nervous system where they serve a dual function:

Abbreviations: VGCCs, Voltage-gated calcium channels; BA, Betulinic acid; DRG, dorsal root ganglia; HVA, high voltage-gated; LVA, low voltage-gated; CaV2.2, N-type voltage-gated calcium channel; CaV3, T-type voltage-gated calcium channel; SNI, spared nerve injury.

* Corresponding author at: Department of Molecular Pathobiology, College of Dentistry, New York University, 433 First Avenue, Room 720, New York, NY 10010, United States.
E-mail address: rk4272@nyu.edu (R. Khanna).
[1] ORCID: 0000-0002-9066-2969.

https://doi.org/10.1016/j.ynpai.2023.100116
Received 20 December 2022; Received in revised form 10 January 2023; Accepted 11 January 2023
Available online 14 January 2023

transduction of membrane potential changes and control of intracellular calcium signaling (Hoppanova and Lacinova, 2022, Lipscombe and Lopez-Soto, 2021). According to the voltage threshold at which they become activated, VGCCs are divided into high-voltage activated (HVA, activated at voltages more positive than −40 mV) and low-voltage-activated (LVA, activated at subthreshold membrane depolarizations between −65 mV and −50 mV) (Guidelli, 2022; Weiss et al., 2012; Felix et al., 2013). The HVA subgroup has seven members, four of them (CaV1.1–1.4) generate L-type currents and the other three (CaV2.1–2.3) produce P/Q-, N-, or R-type currents, respectively. On the other hand, the three members of LVA channels (CaV3.1–3.3) generate T-type currents (Hoppanova and Lacinova, 2022; Weiss et al., 2012).

CaV2.2 channels are expressed in nociceptors at soma and presynaptic terminals. Calcium influx through N-type calcium channels located in the central terminal of primary afferent fibers leads to neurotransmitter release (Zamponi, 2017; Zamponi, 2016), while those expressed in the spinal cord are involved in excitability and central sensitization (Heinke et al., 2004). Recently, CaV2.2 expression was also reported in nerve endings innervating skin, functionally supporting heat hypersensitivity (DuBreuil et al., 2021). As has been reported widely, N-type channels are overexpressed in chronic pain, and the clinical use of the specific blocker Ziconotide (Prialt™) alleviates intractable chronic pain in humans (Gao et al., 2021; Miljanich, 2004; Jiang et al., 2013; Nieto-Rostro et al., 2018; Schmidtko et al., 2010; Zamponi et al., 2015). Furthermore, the FDA approved drug Gabapentin can indirectly regulate the function of CaV2.2 channels by disrupting their trafficking by targeting the α2δ-1 subunit, thus preventing the channels from reaching the active zones of synapses, limiting calcium influx and impacting subsequent transmitter release (Patel and Dickenson, 2016; Bauer et al., 2009; Hoppa et al., 2012).

The function and expression of T-type (CaV3) channels is also upregulated in the primary afferent pain pathway (Hoppanova and Lacinova, 2022; Harding and Zamponi, 2022; Joksimovic et al., 2018). During inflammation and neuropathic pain, CaV3.2 channels support pain signaling by regulating afferent fiber excitability and amplifying the voltage signal (Garcia-Caballero et al., 2014; Heppenstall and Lewin, 2006). When the activity of T-type calcium channel is blocked with TTA-P2, sensory neurons exhibit lower excitability, resulting in pain alleviation (Joksimovic et al., 2018; Lauzadis et al., 2020; Cai et al., 2021). Thus, a polypharmacological approach targeting both N- and T-type calcium channels seems to be an ideal strategy to curb pain. In this regard, our laboratories have embarked on the search for natural products with analgesic properties (Duran et al., 2022; Zhou et al., 2020; Zhou et al., 2019; Shan et al., 2019; Cai et al., 2019; Bellampalli et al., 2019; Calderon-Rivera et al., 2022). Our studies have also focused on deorphanization of the targets of these natural products.

We previously reported that betulinic acid (BA, compound **1**) extracted from the desert lavender plant has anti-nociceptive activity (Shan et al., 2019). This compound inhibited spontaneous excitatory post synaptic currents and depolarization-evoked release of calcitonin gene-related peptide (CGRP) from lumbar spinal cord slices. BA also attenuated paclitaxel-, HIV-, and nerve injury-associated peripheral sensory neuropathy via block of N- and T-type calcium currents (Bellampalli et al., 2019). Considering these findings, in the present study, we utilized the common triterpenoid scaffold of betulinic acid (**1**) and betulin (**2**) to develop twenty-eight structural analogs (**3**–**31**) to improve selectivity and potency against voltage-gated calcium channels. Here we report that the betulinic acid derivative **8** decreased calcium influx in sensory neurons by targeting both N- and T-type calcium channels. Notably, analog **8** had antinociceptive activity in the spared nerve injury and formalin models of pain. Thus, analog **8** represents a novel dual polypharmacological modulator of N- and T-type calcium channels that could be used to develop nonaddictive pain therapeutics.

Materials and methods

Chemical synthesis and characterization of betulinic acid and betulin analogs

The experimental procedures for preparation and quality control (via NMR) of the natural product analogs used in this study are described in the Supplementary Materials.

Animals

Pathogen-free adult female Sprague-Dawley rats (~100 g, Envigo, Placentia, CA) were kept in 12-h light and 12-h dark cycle at 23 ± 3 °C in rooms with controlled humidity. Standard rodent chow and water were available *ad libitum*. All animal use was conducted in accordance with the National Institutes of Health guidelines, and the study was conducted in strict accordance with recommendations in the Guide for the Care and Use of Laboratory Animals of the University of Arizona (Protocol #: 16–141). Animals were housed and bred in the University of Arizona Laboratory Animal Research Center. All efforts were made to minimize animal suffering. Animals were randomly assigned to treatment or control groups for the behavioral experiments. Animals were initially housed three per cage but individually housed after the intrathecal cannulation. All behavioral experiments were performed by experimenters who were blinded to the experimental groups and treatments.

Primary culture of dorsal root ganglion neurons

Lumbar dorsal root ganglia (DRG) were dissected from 100 g *female* Sprague-Dawley rats using procedures as described previously (Bellampalli et al., 2019). Dorsal root ganglia were dissected and placed in sterile DMEM (Cat# 11965; Thermo Fisher Scientific, Waltham, MA) and enzymatically dissociated with collagenase type I (5 mg/mL, Cat# LS004194; Worthington) and neutral protease (3.125 mg/mL, Cat# LS02104; Worthington, Lakewood, NJ) for 50 min at 37 °C under gentle agitation. The dissociated cells were then centrifuged at 800 rpm for 3 min and resuspended in DMEM containing 1 % penicillin/streptomycin sulfate (Cat#15140, Life Technologies), 30 ng/mL nerve growth factor (Cat# N2513, Millipore Sigma), and 10 % fetal bovine serum [HyClone]). The cells were seeded on poly-d-lysine– and laminin-coated 12- or 15-mm glass coverslips and incubated at 37 °C for 24–48 h (Piekarz et al., 2012).

Calcium imaging

In rat DRG neurons, changes in depolarization-induced calcium influx were determined by loading neurons with 3-mM Fura-2AM for 30 min at 37 °C (Cat# F1221; Thermo Fisher, stock solution prepared at 1 mM in DMSO, 0.02 % pluronic acid, Cat#P- 3000MP; Life Technologies, Carlsbad, CA) (Bellampalli et al., 2019). DRG neurons were incubated overnight with 10 μM of test compounds. A standard bath solution containing in mM: 139 NaCl, 3 KCl, 0.8 $MgCl_2$, 1.8 CaCl2, 10Na-HEPES, 5 glucose, pH 7.4, was used. Depolarization was elicited with a 10 *sec* pulse of 40-potassium chloride. Fluorescence imaging was achieved with an inverted microscope, Nikon Eclipse TE2000-U, using an objective Nikon Super Fluor 4X and a Photometrics-cooled CCD camera CoolSNAPHQ (Roper Scientific, Tucson, AZ) controlled by Nis Elements software (version 4.20; Nikon Instruments). The excitation light was delivered by a Lambda-LS system (Sutter Instruments, Novato, CA). The excitation filters (340 ± 5 nm and 380 ± 7 nm) were controlled by a Lambda 10 to 2 optical filter change (Sutter Instruments). Fluorescence was recorded through a 505-nm dichroic mirror at 535 ± 25 nm. Images were taken every ~2.4 s during the time course of the experiment to minimize photobleaching and phototoxicity. To provided acceptable image quality, a minimal exposure time that provided acceptable image

quality was used. Changes in cytosolic calcium were monitored following a ratio of F340/F380, calculated after subtracting the background from both channels.

Whole-cell patch-clamp recordings of calcium currents in acutely dissociated DRG neurons

Recordings were obtained from acutely dissociated DRG neurons as described earlier (Bellampalli et al., 2019). Patch-clamp recordings were performed at room temperature (22–24 °C). Currents were recorded using an EPC 10 Amplifier-HEKA (HEKA Elektronik, Ludwigshafen, Germany) linked to a computer with Patchmaster software. DRG neurons were incubated overnight (~16–24 h) with 20 μM of compound **8** or **18**. DMSO was used as control at 0.1 %.

For total Ca^{2+} and N-type calcium current recordings, the external solution consisted of the following (in millimolar (mM)): 110 N-methyl-D-glucamine, 10 $BaCl_2$, 30 TEA-Cl, 10 HEPES, 10 glucose, 0.001 TTX (pH 7.29 adjusted with NaOH, and mOsm/L = 310). To isolate N-type calcium currents, the following blockers were used: TTX (500 nM, Na^+ channel blocker), Nifedipine (10 μM, L-type calcium channel blocker), ω-agatoxin (200 nM, P/Q-type calcium channel blocker), SNX482 (200 nM, R-type calcium channel blocker), and TTA-P2 (1 μM, T-type calcium channel blocker). Patch pipettes were filled with an internal solution containing (in mM): 150 $CsCl_2$, 10 HEPES, 5 Mg-ATP, and 5 BAPTA, (pH 7.24 adjusted with CsOH, and mOsm/L = 305). Peak calcium current was acquired by applying 200-millisecond voltage steps from −70 to +60 mV in 10-mV increments from a holding potential of −90 mV to obtain the current–voltage (I-V) relation. Steady-state inactivation (SSI) curves were obtained by applying an H-infinity protocol that consisted of 1.5-seconds conditioning pre-pulses from −100 to +30 mV in 10-mV increments followed by a 20-millisecond test pulse to +10 mV.

To isolate T-type specific calcium currents, the bath solution consisted of the following (in mM): 2 $CaCl_2$, 152 TEA-Cl, and 10 HEPES (pH 7.4 adjusted with TEA-OH, and mOsm/L = 310). The intracellular recording solution consisted of (in mM) 135 TEA-Cl, 10 EGTA, 40 HEPES, and 2 $MgCl_2$ (pH 7.2 adjusted with hydrofluoric acid, and mOsm/L = 310). T-type currents were isolated as described before (Choe et al., 2011). Channel current activation was measured from a holding potential (Vh) of −90 mV by applying 500-ms voltage steps (5 mV increments) from −70 to 60 mV. Channel current inactivation was determined by applying a 1500-ms conditioning pre-pulse (-110 to 20 mV in 10 mV increments). The voltage was stepped to −30 mV for 20 ms; a 40-ms interval with a Vh of −90 mV separated each voltage step.

For I-V curves, functions were fitted to data using a non-linear least squares analysis. I-V curves were fitted using double Boltzmann functions:

$$f = a + g_1/\left(1 + exp\left(\left(x - V_{1/2}1\right)/k1\right)\right) + g_2/\left(1 + exp\left(-\left(x - V_{1/2}2\right)/k2\right)\right)$$

where x is the pre-pulse potential, $V_{1/2}$ is the mid-point potential and k is the corresponding slope factor for single Boltzmann functions. Double Boltzmann fits were used to describe the shape of the curve, not to imply the existence of separate channel populations. Numbers *1* and *2* indicate the first and the second mid-points; *a* and *g* are fitting parameters.

Normalization of currents to each cell's capacitance (pF) was performed to get current density. Activation curves were obtained from the I-V curves by dividing the peak current at each depolarizing step by the driving force according to the equation: $G = I/(V_{mem}\text{-}E_{rev})$, where I is the peak current, V_{mem} is the membrane potential and E_{rev} is the reversal potential. The conductance (G) was normalized against the maximum conductance (G_{max}). For total and the different subtypes of calcium currents, steady-state inactivation (SSI) curves were obtained by applying an H-infinity protocol that consisted of 1.5-seconds conditioning pre-pulses from −100 to +30 mV in 10-mV increments followed by a 200-millisecond test pulse to +10 mV. Inactivation curves were obtained by dividing the peak current recorded at the test pulse by the maximum current (I_{max}). Activation curves were fitted with the Boltzmann equation:

$$G/G_{max} = 1/[1 + exp\ (V_{0.5} - - V_m)/k],$$

where G is the conductance in $G = I/(V_m - E_{Ca})$, G_{max} the maximal conductance obtained from the Boltzmann fit under control conditions, $V_{0.5}$ the voltage for half-maximal activation or inactivation, V_m the membrane potential, and k a slope factor.

Steady state inactivation (SSI) was fitted with the equation:

$$I/I_{max} = I/I_{max} = 1/(1 + exp\ ((V - V_{0.5})/k))$$

The reversal potential for I_{Ca} (E_{Ca}) was determined for each individual neuron.

Capacitive artifacts were fully compensated, and series resistance was compensated by ~70 %. Recordings made from cells with greater than a 5 mV shift in series resistance compensation error were excluded from the analysis. All experiments were performed at room temperature (~23 °C).

Cell culture and transient transfection of HEK293T cells

Human embryonic kidney 293 (HEK293T) cells were cultured in DMEM supplemented with 10 % fetal bovine serum and 1 % penicillin/streptomycin sulfate, maintained in standard conditions (5 % CO_2, 37 °C, saturated humidity). Cells were transfected with 4 μg of either of the channel cDNAs that codify for the LVA or 2.5 μg for the HVA α1 pore forming subunit using Lipofectamine 2000 when cell confluence reached 70–90 %. In addition, for the HVA channels 1 μg of α2δ1 and β3 ancillary subunits were co-transfected. Four to six hours after transfection, cells were seeded onto poly-l-lysine–coated coverslips. Positively transfected cells were identified by the fluorescence of co-transfected enhanced green fluorescent protein (0.5 μg). All experiments were performed 36 h after cell transfection.

Whole-cell patch-clamp recordings of calcium currents in transiently transfected HEK293T cells

For electrophysiological recording, the external solution contained (in mM): 105 CsCl, 40 TEA-Cl, 2 $CaCl_2$, 1 $MgCl_2$, and 10 glucose (pH 7.4 adjusted with CsOH, and mOsm/L = 310–315). The internal solution consisted of (in mM): 120 $CsMeSO_4$, 11 EGTA, 2 Mg-ATP, and 10 HEPES (pH 7.4 adjusted with CsOH, and mOsm/L = 240–310). All experiments were conducted at room temperature (22–24 °C). The current–voltage (I–V) relationship was obtained by applying voltage steps from −70 to +60 mV in 10-mV increments from a holding potential of −90 mV. The T-type calcium currents were elicited by a depolarization to −20 or −10 mV for 200-millisecond from a hold potential of −90 mV.

Data were collected by the Patchmaster software in a HEKA EPC-10 USB patch-clamp system. Voltage errors were minimized by using 80 % series resistance compensation. The capacitance artifact was canceled by using the computer-controlled circuitry of the patch-clamp amplifier.

Behavior pain panel

The analgesic potency of compound **8** was analyzed by an in vivo screening tool, ALGOGram™ (ANS Biotech, Riom, France), as was previously reported (Gomez et al., 2022). This platform allowed us to obtain information about the effects of this compound in 5 different pain areas (Acute and tonic pain, inflammatory pain, neuropathic pain, postoperative pain and visceral pain), by comparing their activity on a battery of 10 validated behavioral pain models with an ANS Biotech reference historical database (Table 4). Assessment of the efficacy, and analgesic effects of a single administration (2 μg/rat i.t.) of compound **8** were analyzed in the rat models of: Tail flick test in healthy rats, paw pressure test in healthy rats, acetic acid-induced writhing, formalin test,

Bennett model of peripheral mononeuropathy, oxaliplatin-induced neuropathy, carrageenan-induced mechanical hyperalgesia, kaolin-induced arthritis, Brennan model of incisional pain; and trinitrobenzene sulfonic acid (TNBS)-induced visceral hypersensitivity (Table 4).

Spared nerve injury

Under isoflurane anesthesia (5 % induction, 2 % maintenance in 2 L/min air), skin on the lateral surface of the left hind thigh was incised. The biceps femoris muscle was bluntly dissected to expose the sciatic nerve and its three terminal branches (Decosterd and Woolf, 2000; Cai et al., 2021). The common peroneal and tibial branches of the left sciatic nerve were tightly ligated with 4–0 silk and axotomized 2.00 mm distal to the ligation. The closure of the incision was made in two layers. The muscle was sutured once with 5–0 absorbable suture: skin was auto-clipped. Animals were allowed to recover for 7 days before any testing. SNI-induced allodynia was quantified as percentage of maximum possible allodynia using the formula: percentage allodynia = [(baseline threshold – post-injury threshold)/baseline threshold] X 100. Reversal of allodynia by compound **8**, was quantified with respect to the area under the threshold-time curve (using the trapezoidal method) over the post-injection testing period. Data are reported as percentage of the maximum possible anti-allodynia compared to a hypothetical situation in which the drug brought withdrawal thresholds to their original baseline (day 15 post-surgery).

Testing allodynia

As previously described the assessment of tactile allodynia (defined as a decrease threshold to paw withdrawal after probing with normally innocuous mechanical stimuli) consisted of testing the withdrawal threshold of the paw in response to probing with a series of calibrated fine (von Frey filaments). Each filament was applied perpendicularly to the plantar surface of the rat's paw held in suspended wire mesh cages. Withdrawal threshold was determined by sequentially increasing and decreasing the stimulus strength (the "up and down" method), and data were analyzed with the nonparametric method of Dixon and expressed as the mean withdrawal threshold (Bellampalli et al., 2019; Chaplan et al., 1994).

Data analysis

Graphing and statistical analysis was performed with GraphPad Prism (Version 9). All data sets were checked for normality using D'Agostino & Pearson test. Details of statistical tests, significance and sample sizes are reported in the appropriate table (see Table S1). All data plotted represent mean ± SEM.

Results

Ratiometric screening of betulinic acid derivatives on depolarization-evoked calcium influx in rat DRG neurons

We previously reported that 20 μM of betulinic acid (BA, **1**) extracted from the desert lavender *H. emoryi*, inhibited ~90% of depolarization-evoked calcium influx in rat dorsal root ganglia (DRG) neurons (Gomez et al., 2022). Because of its promising antinociceptive activity, additional derivatization studies were carried out to identify BA derivatives with even greater selectivity and potency against calcium channels. With this in mind, a collection of twenty-eight new molecules were chemically synthesized (Figs. S1–32) modifying the R1, R2, and R3 groups of the pentacyclic triterpenoid structure of betulinic acid (**1**) and its naturally-occurring analog betulin (**2**).

To first test the functional effect of the betulinic acid and betulin derivatives **3**–**31** on depolarization-evoked calcium influx, a lower concentration of compounds was used for the calcium imaging experiments (10 μM instead of the 20 μM previously used (Bellampalli et al., 2019). Primary rat DRG neurons seeded on coverslips were treated overnight with 10 μM of the indicated compounds or 0.1 % DMSO as a vehicle (negative) control. The following day, DRG neurons were loaded with Fura2-AM for 30 min before being mounted in a perfusion chamber for the imaging assay. To evoke the activity of calcium channels, 40 mM KCl was used in the bath and the resulting calcium influx following the depolarization stimulus was measured at the peak (Fig. 1) (Gomez et al., 2022). When compared to DMSO, betulinic acid (**1**) at 10 μM inhibited depolarization-evoked calcium influx by ~50 % (Fig. 1). This represents a ~40 % reduction in inhibition when compared to incubation with 20 μM of compound **1** (Gomez et al., 2022). Seven compounds, including betulinic acid analogs **4**, **8**, **9**, **14**, and betulin analogs **18**, **20**, and **24** demonstrated more than 50 % inhibition (underlined in Fig. 1). Three of these – **8**, **14**, and **18** – exhibited robust inhibition of ~65 % (Table S1 lists statistical tests and significance values for all data). Due to the strongest inhibitory effect in the depolarization-evoked calcium influx assay, we selected betulinic acid analog **8** and betulin analog **18** for further investigation. Analog **14** was not explored further as it shares the same substituents on the triterpene scaffold, except for the epoxy group in the sided-chain, which makes it more structurally related to **1**.

Analog 8, but not 18, diminishes total calcium currents in DRG neurons

Voltage-gated calcium channels (VGCCs) are functionally expressed in DRG neurons where they drive cell signaling functions. To investigate whether currents through these VGCCs are modulated by compounds **8** and **18**, we performed whole-cell patch-clamp recordings on isolated small-to-medium diameter rat DRG neurons. As we previously reported, overnight incubation with 20 μM of betulinic acid inhibited the activity of VGCCs (Bellampalli et al., 2019). Because compounds **8** and **18** are BA-analogs, DRG neurons were incubated in the same comparable conditions (20 μM and overnight incubation) before proceeding with the recordings. Fig. 2A shows representative family of traces from DMSO and compound treated neurons - the amplitude of total calcium currents in DRG neurons pre-treated with **8**, but not **18,** were smaller compared to the control condition (0.1 % DMSO). To account for cell size differences, the current amplitude was normalized to the cell size and the subsequent current density was plotted versus the voltage applied (Fig. 2B). Both the current density (Fig. 2B) and the peak current (Fig. 2C) show a ~55 % of reduction in the voltage-dependent calcium influx in the presence of analog **8**, while no change was observed with analog **18**. Neither analog **8** nor analog **18** affected the half-activation voltage where 50 % of the maximal conductance level is reached ($V_{1/2}$) or the slope (k) of the steady-state inactivation and activation curves (Fig. 2C and Table 1). These results show that compound **8** inhibits total voltage-dependent calcium currents, similar to the findings observed with betulinic acid (Bellampalli et al., 2019). Since analog **8** affected the activity of VGCCs, we next interrogated if this compound affected specific subtypes of channels, focusing on N- and T-type calcium channels, the reported targets of betulinic acid (Bellampalli et al., 2019).

Betulinic acid analog 8 inhibits N-type calcium currents

N-type calcium channels are expressed in small-to-medium diameter rat DRG neurons where they are the major component of the total calcium current (~70 %) (Scroggs and Fox, 1992). Changes in CaV2.2 function and expression in the pain pathway after nerve injury, inflammatory and postoperative pain have been reported (Murali et al., 2015; François-Moutal et al., 2015; Bell et al., 2004). Because betulinic acid (**1**) acts on N-type channels and because compound **8** has a high structural resemblance to betulinic acid (**1**), we tested whether analog **8** could also affect N-type calcium currents. N-type currents were pharmacologically isolated with a cocktail of channel blockers in the external solution, including Nifedipine (L-type calcium channel blocker),

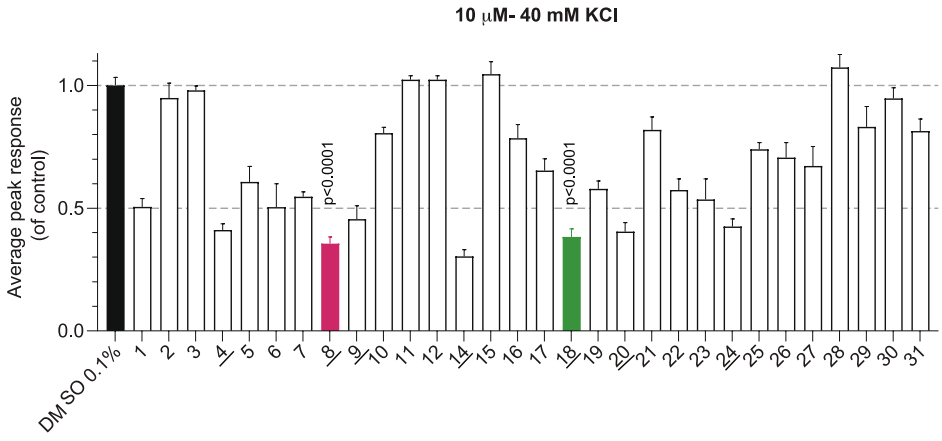

Fig. 1. Effect of betulinic acid and betulin analogs on depolarization-evoked calcium influx in rat DRG sensory neurons. Peak calcium responses of female DRG sensory neurons incubated overnight with 0.1 % DMSO (vehicle) or 10 μM of BA analogs in response to 40-mM KCl. Betulinic acid (**1**) was used as a control (n = 33–365 neurons). The underlined compounds demonstrated more than 50 % inhibition in comparison to vehicle (0.1 % DMSO)-treated controls. Average responses were normalized to that of the vehicle and are shown as mean ± SEM. One-way ANOVA with Dunnett's post-hoc test (see Table S1 for full statistics).

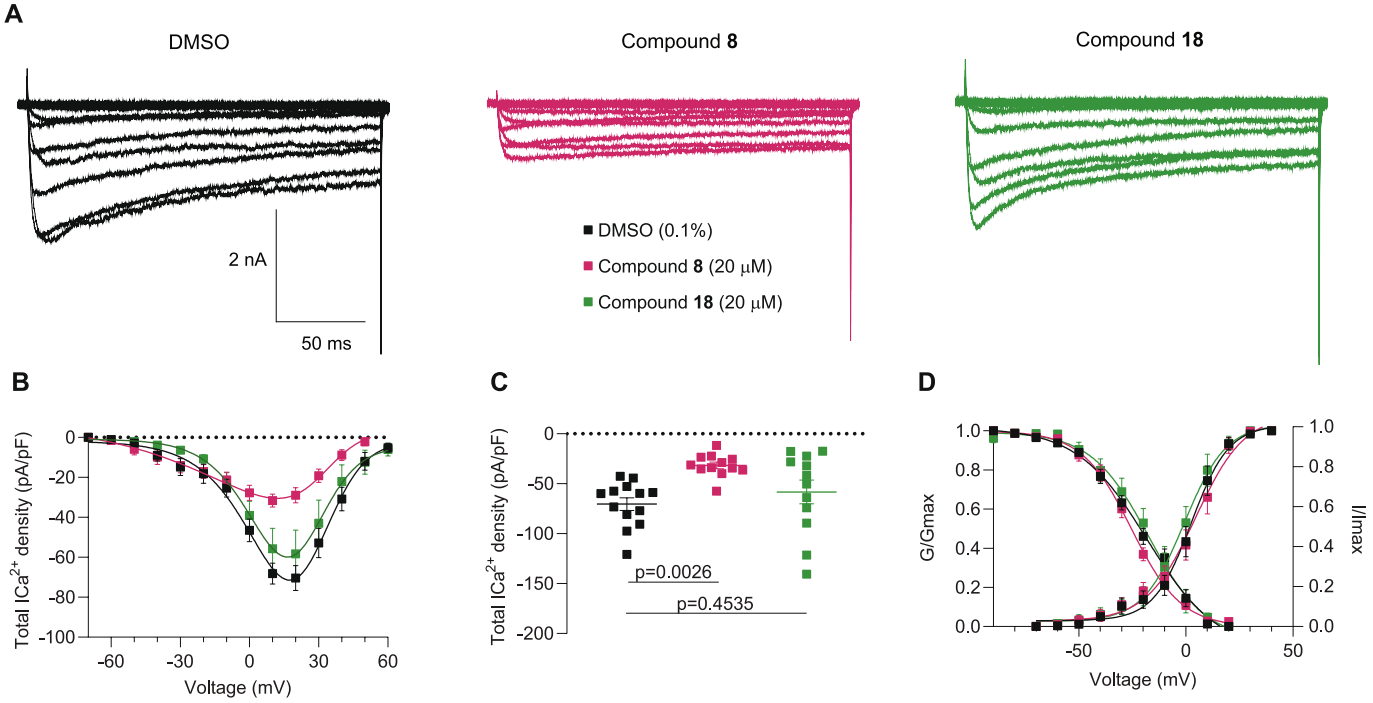

Fig. 2. Total calcium currents are inhibited by betulinic acid analog **8** in isolated dorsal root ganglia. (A) Representative family of total calcium currents recorded from small- to medium-sized DRG neurons from female rats. (B) Current density–voltage relationship of control (0.1 % DMSO), analogs **8** and **18** evoked from −70 to +60 mV for 200-milliseconds. (C) Summary showing peak calcium current density (DMSO −70.4 ± 6.3, **8**–31.7 ± 3.2, **18**–58.3 ± 11.9). (D) Boltzmann fits for voltage dependence activation and inactivation. Table 1 summarizes the half-maximal activation potential of activation and inactivation ($V_{1/2}$) and slop values (k) for voltage-dependence activation and inactivation. n = 12–13 cells: error bars indicate mean ± SEM; p values as indicated, one-way ANOVA with Tukey's post hoc test (see Table S1 for full statistics).

ω-agatoxin (P/Q calcium channel blocker), SNX482 (R-type calcium channel blocker), and TTA-*P*2 (T-type channel blocker; See methods for details). DRG neurons were incubated overnight with analog **8** at 20 μM or 0.1 % DMSO. Fig. 3A shows representative traces of N-type channels with lower current amplitude when neurons were treated with analog **8** compared to DMSO. Current density–voltage relationship and peak current density are shown in Fig. 3B and 3C and demonstrate that analog **8** reduced N-type current density by ~56 % when compared to the control condition. Analog **8** did not modify the corresponding Boltzmann parameters of ($V_{1/2}$) or the slope (k) of activation or inactivation (Fig. 3D and Table 2).

Analog 8 inhibits T-type calcium currents.

Since T-type Ca^{2+} channels are important mediators of DRG neuron excitability, we next tested the ability of compound **8** to block currents via these channels (Choe et al., 2011; Cai et al., 2019). From a holding potential of −90 mV, 200-ms depolarization steps (from −70 to 0 mV in 5 mV increments) were used to evoke T-type calcium currents (See Methods for details). Representative family of T-type Ca^{2+} currents are shown in Fig. 4A. Both the current density–voltage relationship and corresponding peak density (Fig. 4B and 4C) showed an ~ 40 % reduction when compared to DMSO-treated cells. The resulting Boltzmann parameters ($V_{1/2}$) or the slope (k) reported in Table 3 remain unaffected, except for a ~8 mV shift toward depolarization potentials in the $V_{1/2}$ of activation in neurons recorded in the presence of analog **8** (see Fig. 4D). This 8-mV shift suggests that the stochastic influx of calcium through the T-type calcium channels at voltages near the resting membrane potential is lower in the presence of analog **8** (Liu et al., 2019; Liu et al., 2019). Notably, no effect of analog **8** was seen upon acute

Table 1
Gating properties of total calcium currents recorded from DRG neurons.[a]

Total Ca^{2+}	DMSO	Compound **8**	Compound **18**
Activation			
$V_{1/2}$	0.8 ± 1.4 (9)	1.8 ± 2.0 (6) p = 0.904	1.8 ± 2.2 (7) p = 0.896
k	8.1 ± 1.2 (9)	10.6 ± 1.8 (6) p = 0.468	8.0 ± 2.0 (7) p = 0.997
Inactivation			
$V_{1/2}$	−21.9 ± 1.6 (9)	−25.1 ± 1.0 (10) p = 0.187	−22.7 ± 1.7 (7) p = 0.89
k	−13.6 ± 1.5 (9)	−9.8 ± 0.9 (10) p = 0.075	−10.6 ± 1.5 (7) p = 0.232

[a] Values are mean ± SEM calculated from fits of the data from the indicated number of individual cells (in parentheses) to the Boltzmann equation: $V_{1/2}$ midpoint potential (mV) for voltage dependence of activation or inactivation; and *k* slope factor. These values correspond to data shown in Fig. 2. No statistical differences were observed when compared with the control (DMSO). Data were analyzed with one-way ANOVA with Dunnett's post hoc test. Abbreviations: DRG, dorsal root ganglia: DMSO, dimethyl sulfoxide.

treatment of HEK293T cells transiently transfected with CaV3.1, CaV3.2 or CaV3.2 channels (Fig. S33). Therefore, these data suggest that rather than a direct block of T-type Ca^{2+} channels, compound **8** could indirectly modulate these channels and decrease their activity in DRG neurons.

Compound 8 reduces calcium currents through CaV2.2 and CaV3.2 channels in heterologously expressed cells

To get further evidence of the potential selectivity of analog **8**, we next tested it in HEK293T cells transiently transfected with the HVA channels CaV1.2, CaV1.3 and CaV2.2, co-transfected with the ancillary subunits α2δ1 and β3 as well as on the LVA CaV3.1, CaV3.2 or CaV3.3 α1 subunits, which were transiently expressed alone. Whole cell patch clamp recordings showed that the recombinant L-type currents through CaV1.2 and CaV1.3 channels were not affected by an overnight incubation with compound **8** (Fig. 5A). When CaV2.2 channels were expressed in this cellular milieu, its activity was robustly reduced by analog **8** (Fig. 5B). Fig. 5C shows analog **8** also inhibited CaV3.2 (by ~45 %), but not CaV3.1 and CaV3.3, T-type currents. Collectively, the results from these heterologous cells show that compound **8** modulates calcium current through a specific block of CaV2.2 and CaV3.2 channels.

Table 2
Gating properties of N-type (CaV2.2) calcium currents recorded on DRG neurons.[a]

N-type Ca^{2+}	DMSO	Compound **8**	p value
Activation			
$V_{1/2}$	2.1 ± 0.6 (11)	2.2 ± 1.7 (8)	0.931
k	5.6 ± 0.6 (11)	8.2 ± 1.5 (8)	0.134
Inactivation			
$V_{1/2}$	−24.3 ± 2.4 (11)	−20.2 ± 3.6 (8)	0.37
k	−17.6 ± 2.5 (11)	−17.4 ± 3.5 (8)	0.966

[a] Values are mean ± SEM calculated fitting the data from the indicated number of individual cells (in parentheses) to the Boltzmann equation: $V_{1/2}$ midpoint potential (mV) for voltage dependence of activation or inactivation; and *k* slope factor. These values correspond to data shown in Fig. 3. No statistical differences were observed between groups. Data were analyzed with *t*-test with Welch's correction. Abbreviations: DRG, dorsal root ganglia: DMSO, dimethyl sulfoxide.

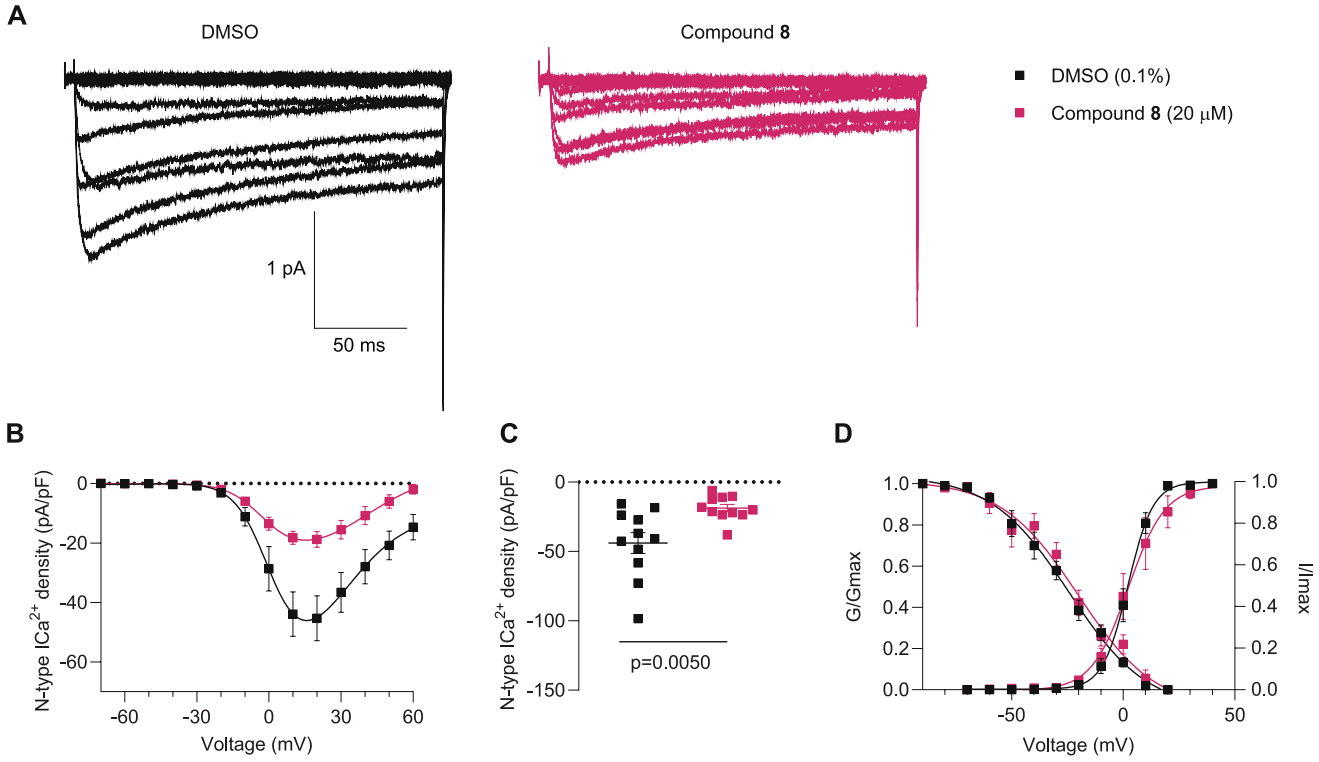

Fig. 3. Analog **8** inhibits N-type (Cav2.2) calcium currents in dorsal root ganglia neurons. (A) Representative family of N-type calcium currents evoked by voltage steps from −70 to +60 mV for 200-milliseconds. (B) Current-voltage relationship of control (0.1 %-DMSO), compound **8**, evoked from −70 to +60 mV for 200-milliseconds. (C) Peak calcium current density summarized as scatter plots (DMSO −44.0 ± 7.52 (n = 11), **8** −18.8 ± 2.7 (n = 10)). (D) Steady-state inactivation and activation curves. To evaluate steady-state inactivation, currents were elicited by a 20 ms pulse at 10 mV after a 1500 ms pre-pulses ranging from −100 mV to 30 mV in 10 mV increments from a holding potential of −60 mV. Table 2 summarizes the half-maximal activation potential of activation and inactivation ($V_{1/2}$) and slop values (*k*) for voltage-dependence activation and inactivation. n = 10–11 cells; error bars indicate mean ± SEM; p values as indicated (see Table S1 for full statistics).

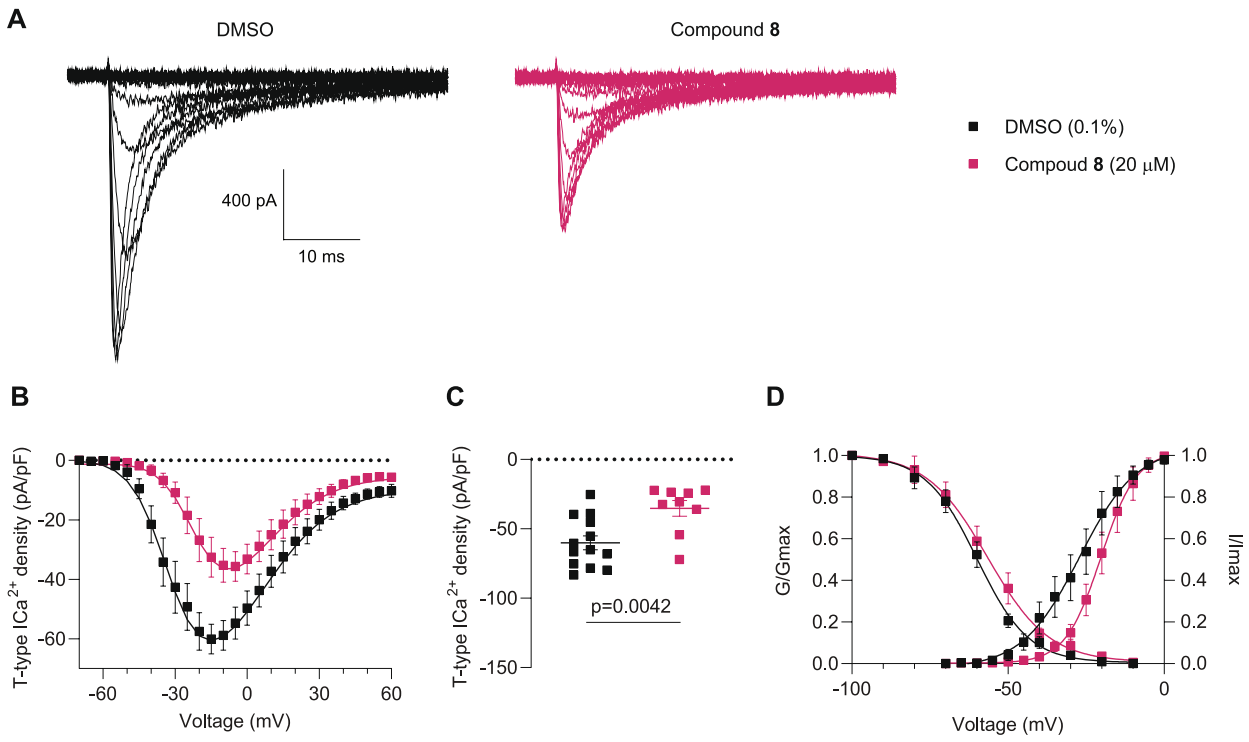

Fig. 4. T-type calcium currents are reduced by compound **8**. (A) Representative T-type Ca^{2+} current traces evoked by voltage steps from −70 to 0 mV in increments of 5 mV. (B) Average current density–voltage plot of control (0.1 % DMSO) and compound **8** (20 μM). Currents were measured from a holding potential of −90 mV with voltage steps of 200 ms of duration applied at 0.5 s intervals in 5 mV increments (C) Peak current density summarized as scatter plot (0.1 %-DMSO, −60.1 ± 5.0, compound **8**–35.3 ± 5.7). (D) Boltzmann fits for and steady-state inactivation curves. After a 1.5 s pre-pulses ranging from −100 mV to −10 mV in 10 mV increments from a holding potential of −90 mV. Half-maximal activation potential of activation, inactivation ($V_{1/2}$) and slope values (k) for activation and inactivation are presented in Table 3. n = 9–13 cells; error bars indicate mean ± SEM; p values as indicated (see Table S1 for full statistics).

Table 3
Gating properties of T-type calcium currents recorded on DRG neurons.[a]

T-type Ca^{2+}	DMSO	Compound **8**	p value
Activation			
$V_{1/2}$	−27.1 ± 2.0 (10)	−20.2 ± 1.0 (8)	0.007
k	9.2 ± 1.9 (10)	5.7 ± 0.85 (8)	0.113
Inactivation			
$V_{1/2}$	−59.9 ± 1.1 (10)	−56.5 ± 1.6 (8)	0.098
k	−8.2 ± 1.0 (10)	−9.8 ± 1.6 (8)	0.404

[a] Values are mean ± SEM calculated from fits of the data from the indicated number of individual cells (in parentheses) to the Boltzmann equation: $V_{1/2}$ midpoint potential (mV) for voltage dependence of activation or inactivation; and k slope factor. These values correspond to data shown in Fig. 4. No statistical differences were observed between groups except for $V_{1/2}$ of activation. Data were analyzed with t-test with Welch's correction. Abbreviations: DRG, dorsal root ganglia: DMSO, dimethyl sulfoxide.

Analog 8 reverses mechanical allodynia in the spared nerve injury model

Since the overall effect of blocking N- and T-type Ca^{2+} channel can result in amelioration of pain behaviors, we hypothesized that compound **8** could reverse nociception in a neuropathic pain model. The spared nerve injury model was selected because it robustly displays persistent and relatively localized mechanical allodynia (Decosterd and Woolf, 2000; Muralidharan et al., 2020). As shown in Fig. 6A, in rats experiencing mechanical allodynia following SNI, intrathecal administration of analog **8** (2 μg in 5 μl) significantly increased paw withdrawal thresholds (PWTs), reaching a peak effect 3 h after its delivery. Moreover, the area under the curve was also increased in rats treated with **8** (Fig. 6B). These findings indicate that the betulinic acid analog **8** has antinociceptive activity.

Analog 8 reverses nociceptive behaviors in experimental models of acute and tonic formalin test

ANS biotech, a preclinical contract research organization exclusively dedicated to the pharmacology of pain independently tested analog **8** to establish whether this compound has analgesic efficacy in other pain models (Darbaky et al., 2017; Gris et al., 2016; Silos-Santiago et al., 2013). In their patented pain screen ALGOGram™, the potential antinociceptive and analgesic activities of compound **8** was tested in ten validated preclinical rodent models within the areas of acute and tonic pain, neuropathic pain, inflammatory pain, post-operative pain, and visceral pain (Table 4 and Fig. S34) (Gomez et al., 2022). The percentage of analgesic activity of **8** against the vehicle group was compared to an ANS Biotech certified confidential internal reference, which varies according to the pain model used (Table 4). We previously reported that **1** reached maximum antinociceptive effect 2 h after administration in the partial sciatic nerve ligation (pSNL), chemotherapy-induced peripheral neuropathy (CIP), and HIV-induced sensory neuropathy (HIV-SN) models of experimental pain. Therefore, based on these results, we chose a time point of 2 hr to measure the effect of analog **8** (2 μg/rat, i.t.) in the *in vivo* set of preclinical models assessed by ANS Biotech.

In healthy rats (without pain), paw pressure and tail flick tests showed that a single administration of compound **8** preserved acute mechanical and thermal sensitivity (-5.5 % and 0.5 % of analgesic activity, respectively). These parameters are strongly altered in the presence of the internal reference morphine (66–67 % effect). Therefore, the baseline nociceptive thresholds did not change when analog **8** was administered.

In the acetic acid test (0.6 % acetic acid, parenterally administered), characterized by abdominal writhing movements in rats, the analgesic

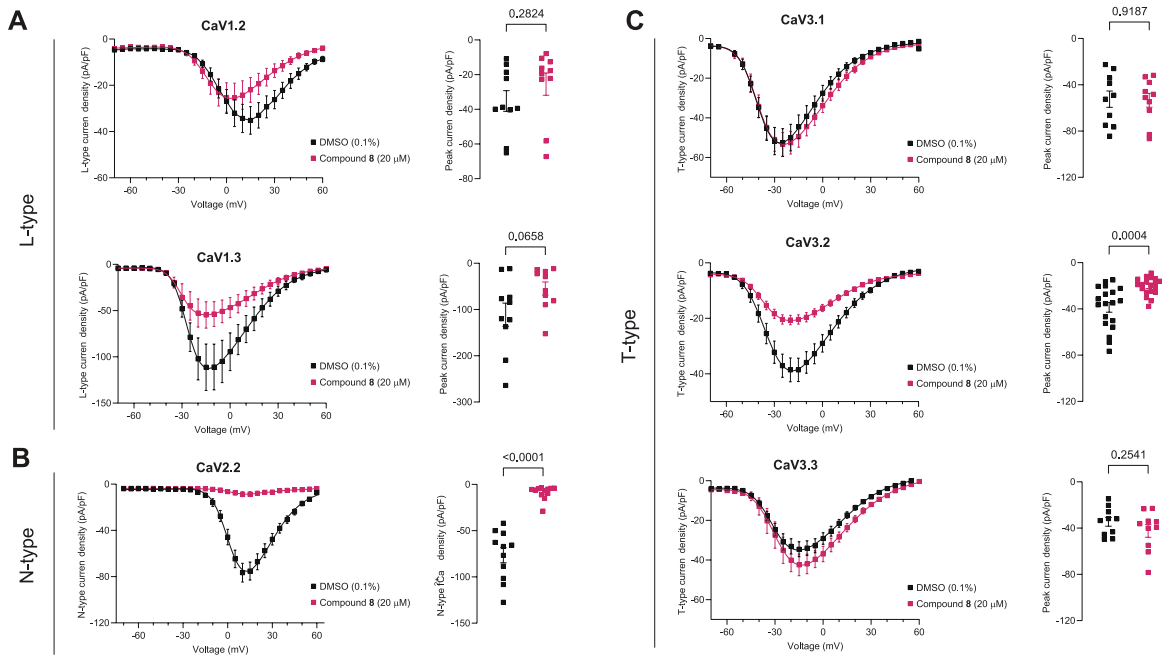

Fig. 5. Compound **8** reduces calcium current through CaV2.2 and CaV3.2 channels expressed in HEK cells. Current density–voltage relationships from HEK cells transiently transfected with plasmid constructs encoding CaV1.2 and CaV1.3 channels (A left), CaV2.2 channels (B left); CaV3.1, CaV3.2, and CaV3.3 channels (C, left). The corresponding peak current densities are shown on the right of each I-V plot. Black symbols indicate overnight incubation with 0.1 % DMSO (control condition). Pink symbols indicate cells treated overnight with 20 μM of compound **8**. p values as indicated, Student's *t*-test.

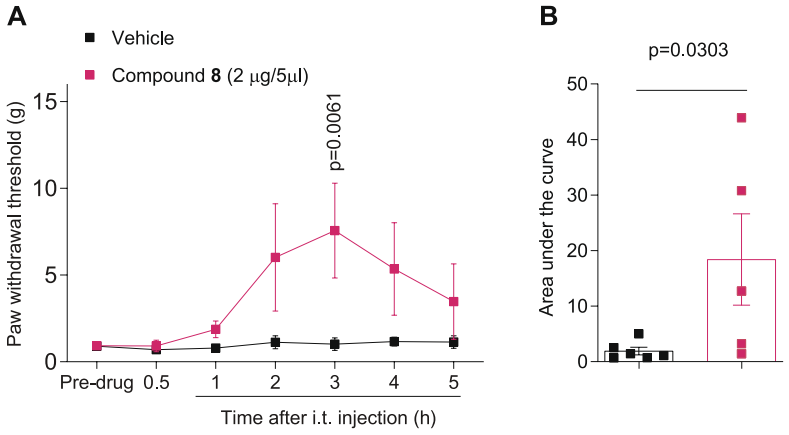

Fig. 6. Betulinic acid analog **8** is antinociceptive 3 h after intrathecal delivery. Time course (A) and quantification (B) of paw withdrawal threshold (PWT) of male rats with neuropathic pain induced by spared nerve injury (SNI). At 14 days following SNI, analog **8** was intrathecally administered (2 μg in 5 μl). Compound **8** produced antinocieption 3 h following injection (vehicle 18.4 ± 8.2 (n = 6), analog **8** 1.9 ± 0.7 (n = 5)). *p* values as indicated, two-way ANOVA with Mann-Whitney post hoc test (see Table S1 for full statistics). The behavioral experiments were performed by an experimenter who was blinded to the experimental groups and treatments.

activity of analog **8** was 24.5 % (internal reference and % of analgesic activity: (−) U50, 488 H, 100 %).

The antinociceptive effect of compound **8** was tested in a model of persistent pain induced by 2.5 % Formalin (Shields et al., 2010). Administration of compound **8** in this model produced 31.5 % and 45.5 % analgesic activity in the early and late phases, respectively (internal reference: morphine with 65 % in early phase and 77 % in late phase). It has been suggested that the early phase (also called short phase) seems to be caused mainly by activation of nociceptors produced by discharge of nociceptive nerves, while the late phase appears to be due to the functional changes occurring in the dorsal horn of the spinal cord and/or inflammatory sensitization of nerve endings (Tjolsen et al., 1992).

The model of chronic constriction injury (Bennett model) was used to assay the effect of analog **8** in neuropathic pain. In this model, compound **8** displayed modest anti-analgesic activity (−20 %) compared to the vehicle-treated group (internal reference and % of analgesic activity: morphine, 188 %). Moreover, in the oxaliplatin-induced peripheral neuropathy model (10 mg/kg oxaliplatin) (51), the effect was −2% (internal reference and % of analgesic activity: duloxetine, 66 %). In addition, in the inflammatory pain model induced by intraplantar injection of 2 % carrageenan, the analgesic activity was 2 % (internal reference and % of analgesic activity: indomethacin, 92 %). However, in a model of arthritis induced by 10%-kaolin, analog **8** was not efficacious (−13 % of analgesic activity: internal reference and % of analgesic activity: indomethacin, 64 %). On the other hand, compound **8** had a slight analgesic activity in the Brennan model of post-operative pain (Brennan et al., 1996) and in the 2,4,6-Trinitrobenzenesulfonic acid (TNBS)-induced visceral pain model (50 mg/kg) (Darbaky et al., 2017; Silos-Santiago et al., 2013) (11% and 6.5% of analgesic activity: internal reference and % of analgesic activity: morphine, 107 %: and (−) U50, 488H, 168%). Individual raw data is available in Fig. S34. These results show that analog **8** has antinociceptive effect across a breadth of pain models with decreasing percent efficacies: Formalin test late phase (45.5%) > formalin test early phase (31.5%) > acetic acid test (24.5%) > Brennan model (11%) > TNBS (6.5%) > Carrageenan (2%).

Table 4
Effect of a single administration (2 μg/rat i.t.) of compound 8 in ALGOGram.[a]

Pain area	Model (test)	Compound **8**	Internal reference	
		Percentage of analgesic activity vs vehicle	Reference ID	Percentage of activity vs vehicle
Acute and tonic pain	Healthy rats (paw pressure test)	−5.5 %	Morphine, 4 mg/kg s.c., T30 min	67 %
	Healthy rats (tail flick test)	0.5 %	Morphine, 4 mg/kg s.c., T30 min	66 %
	Acetic acid test (abdominal cramps)	24.5 %	(-) U50, 488H, 4 mg/kg s.c., T30 min	100 %
	Formalin test (paw licking time early phase)	31.5 %	Morphine, 4 mg/kg s.c., T30 min	65 %
	Formalin test (paw licking time late phase)	45.5 %	Morphine, 4 mg/kg s.c., T30 min	77 %
Neuropathic pain	Bennett model (Paw pressure test)	−20 %	Morphine, 3 mg/kg s.c., T30 min	188 %
	Oxaliplatin (paw immersion test)	−2%	Duloxetine 100 mg/kg, p.o., T60 min	66 %
Inflammatory pain	Carrageenan (paw pressure test)	2 %	Indomethacin 30 mg/kg, p.o., T60 min	92 %
	Kaolin (Gait score)	−13 %	Indomethacin 30 mg/kg, p.o., T60 min	64 %
Post-operative pain	Brennan model (Electronic Von Frey test)	11 %	Morphine, 4 mg/kg s.c., T30 min	107 %
Visceral pain	TNBS (colonic distension)	6.5 %	(-) U50, 488H, 4 mg/kg s.c., T30 min	168 %

[a] Testing: 120 min after treatment. n = 4/model/test. Results are expressed for each group as percentage of activity calculated from the mean value of the vehicle-treated animals and compared to naïve animals, control paw or cut-off value depending on the test (from the ANS Biotech historical database (Darbaky et al., 2017; Gris et al., 2016; Silos-Santiago et al., 2013). All experiments were done in a blinded manner.

Discussion

Capitalizing on our previous report of the analgesic activity profile of betulinic acid (BA, **1**) (Bellampalli et al., 2019), in this study we synthesized twenty-eight pentacyclic triterpene analogs of BA and betulin (**2**) to increase potency and efficacy. Of the compounds screened in multiple *in vitro* orthogonal assays, we report compound **8**, a BA analog, as preferentially inhibiting N-type (CaV2.2) and T-type (CaV3.2) type voltage-gated calcium channels. In vivo screening demonstrated that compound **8** has potent antinociceptive activity in both formalin and spared nerved injury (SNI) models of pain.

BA possesses three sites that are highly adaptable to substitution, including the C-3 hydroxyl, C-20 alkene, and C-28 carboxylic acid positions. Fifteen of the twenty-eight analogs were derived from betulinic acid (**1**) while thirteen were betulin (**2**) analogs. Analogs **8** and **18** showed strong inhibition of depolarization evoked calcium influx, slightly superior to **1**, in DRGs. However, from recordings of total calcium currents in DRG neurons with analogs **8** and **18**, only compound **8** inhibited the current (~55 %), when compared with the vehicle-treated cells. This reduction is similar to the ~51 % produced by betulinic acid (compound **1**) (Bellampalli et al., 2019). Moreover, the N-type current in DRG neurons was likewise (~56 %) decreased by compound **8**. The inhibition imposed by analog **8** on CaV2.2 expressed in HEK293 cells was >95 %, likely explained due the combination in the composition of the ancillary subunits forming the functional channel, the specific splice variant expressed, and/or lack of adequate number of γ-subunits, or intracellular regulatory proteins. Compound **8** also inhibited T-type currents from DRG neurons by ~40 %, slightly lower than the ~50 % inhibition we previously reported with compound **1** (Bellampalli et al., 2019). When the activity of CaV3.1-CaV3.3 T-type isoforms, expressed in HEK293 cells, was interrogated, compound **8** showed a preference in blocking the activity of CaV3.2 channels over CaV3.1 and CaV3.3 channels. In contrast to the parent compound betulinic acid (**1**) which caused acute inhibition of transiently expressed channels (Bellampalli et al., 2019), no inhibition was observed with acute treatment with compound **8**. This finding suggests compound **8** likely works indirectly to affect CaV3.2 channels, likely an effect on channel trafficking or stability, reminiscent of the mechanism of action of gabapentinoids on α2δ subunit of calcium channels (Alles and Smith, 2017).

Both CaV2.2 and CaV3.2 channels have been demonstrated to be important contributors to nociceptive signal transduction. CaV3.2 is primarily involved in signal conductance along nociceptive neurons, whereas CaV2.2 is primarily involved in synaptic transmission at the dorsal horn (5). CaV2.2 channel expression predominates in DRG neurons over other members of the VGCC family (Ramachandra et al., 2013). Strong evidence supports a role for CaV2.2 in pain transmission (Evans et al., 1996). CaV2.2 knockout mice demonstrated markedly reduced responses in the phase 2 of the formalin test, indicating suppression of inflammatory pain (Saegusa et al., 2002) as well as show reduced symptoms of neuropathic pain after spinal nerve ligation (Saegusa et al., 2002). Spinal antagonism of CaV2.2 by the synthetic version of the conotoxin peptide ziconotide ameliorates severe pain conditions (Zamponi et al., 2015). The CaV2.2 channels are also indirectly inhibited by the gabapentinoids – gabapentin and pregabalin, both of which are ligands of the auxiliary α2δ subunits of these channels – and are used to treat neuropathic pain, diabetic neuropathy, and postherpetic and trigeminal neuralgia (Zamponi et al., 2015).

In addition to N-type VGCCs, T-type channels are crucial molecular targets for the treatment of pain (Bourinet et al., 2014; Todorovic and Jevtovic-Todorovic, 2011; Weiss and Zamponi, 2019). CaV3.2 is functionally expressed in the soma of medium, and small size DRG neuros (Scroggs and Fox, 1992; Nelson and Todorovic, 2006; Schroeder et al., 1990; Nelson et al., 2005). It has been reported that ~30–40 % of all CaV3.2-positive DRG neurons in mice and 20 % in rats express calcitonin gene-related peptide (CGRP) (Rose et al., 2013). Small depolarizations in DRGs can activate T-type currents via CaV3.2 channels and release CGRP (Jacus et al., 2012). In the model of formalin, analog **8** was intrathecally applied, suggesting that it may be inhibiting the transmission of the sensory information in the spinal cord. As we previously reported, BA inhibited sEPSC frequency, but not amplitude, supporting a presynaptic mechanism of action.

Electrophysiological, pharmacological, molecular, and genetic approaches support the role of T-type currents, and particularly CaV3.2 channels in nociception. The activity and expression of CaV3.2 channels is increased in DRG neurons and in the spinal dorsal horn during painful pathological conditions, including chronic constriction injury (CCI), L5/L6 spinal nerve ligation (SNL), partial sciatic nerve ligation, spared nerve injury (SNI), and diabetic neuropathy (Harding and Zamponi, 2022; Cai et al., 2021). In both inflammatory and neuropathic pain mice models, T-type currents are inhibited by blockers like mibefradil,

ethosuximide, NNC 55-0396, Z944 and TTA-P2 (Joksimovic et al., 2018; Lauzadis et al., 2020; Cai et al., 2021; Choe et al., 2011; Lee, 2014). However, randomized clinical trials using the established T-type channel blockers ethosuximide and ABT-639 failed to meet clinical endpoints in reducing pain and several adverse events were reported (Kerckhove et al., 2018; Wallace et al., 2016; Ziegler et al., 2015). It has been proposed that the low-threshold property of activation makes these channels an important factor in the initial membrane depolarization prior to sodium spikes, which leads to burst firing and oscillatory behavior in the thalamus (Perez-Reyes, 2003).

From the calcium imaging results, 40 mM-KCl depolarizes the membrane close to −30 mV (estimated by the Nernst equation), at this concentration the activation of low voltage-gated calcium channels is expected. Moreover, the voltage-dependence of steady-state activation and inactivation are important electrophysiological correlates of T-type calcium channels that influences neuronal excitability (Nelson et al., 2005; Dreyfus et al., 2010; Jagodic et al., 2007). The overlap of activation and inactivation curves generates a window current, which allows passive calcium influx that contributes to the maintenance of the resting membrane potential (Dreyfus et al., 2010). This changes in pathological states, for example, the activation curve was reported to be hyperpolarized in rat DRG neurons with neuropathic pain (Liu et al., 2019; Liu et al., 2019). According to our findings, in DRG neurons, the depolarizing shift in the voltage dependence of activation ($V_{1/2}$) on T-type currents treated with compound **8** may reduce the passive calcium entry near the resting membrane potential. Together, the smaller T- and N-type calcium currents recorded from DRG neurons could explain the antinociceptive effect of **8**, as this would influence the excitability threshold of DRGs.

Given the structural similarities among the different isoforms of VGCCs, discovery of drugs, small molecules, or natural products that selectively target one subtype has, so far, proven difficult. Identification of VGCC inhibitors that target more than one isoform has been investigated by us and others (Shan et al., 2019; Bellampalli et al., 2019). In the early 1990′s, it was reported that Flunarizine, one of the most often used treatments for migraine, potently inhibits T-type calcium channels but also N- and L-type calcium channels (Tytgat et al., 1988, 1991; Tytgat et al., 1996). Similarly, an *ortho*-phenoxyanilide derivative, MONIRO-1, inhibits human CaV2.2-, CaV3.2- and CaV3.1-mediated currents in HEK293 cells (McArthur et al., 2018). Besides betulinic acid, other natural products derived from plants with analgesic properties have shown to target multiple VGCCs. For example, gossypetin, a flavonoid isolated from *Hibiscus sabdariffa* produces dose-dependent and long-lasting mechanical anti-hyperalgesia that is attenuated in CaV3.2 null mice and works by indirectly modulating CaV3.2 channel stability (Gadotti et al., 2015). Physalin F, a steroidal derivative isolated from the herb Physalis acutifolia, alleviates pain induced by Complete Freund's adjuvant, paclitaxel, and nerve ligation, by inhibiting N-type and R-type calcium channels in DRG neurons (Shan et al., 2019). Moreover, Lavender oil reduces calcium influx through different types of VGCCs such as N-type, P/Q-type and T-type calcium channels (Calderon-Rivera et al., 2022), resulting in alleviation of neuropathic pain induced by SNI (Sanna et al., 2019). This evidence suggests that engaging more than one VGCC can be beneficial for treating inflammatory and neuropathic pain, espousing yet again the importance of a polypharmacological or network pharmacology approach.

In summary, the synthesis and functional characterization of the betulinic acid analogs reported here broaden our understanding of pentacyclic triterpenoid analogs with analgesic properties and point to its structure as a potential platform candidate for developing drugs with anti-nociceptive activity due to their ability to target voltage-gated calcium channels implicated in pain.

CRediT authorship contribution statement

Aida Calderon-Rivera: Methodology, Formal analysis, Investigation, Writing – original draft. **Kimberly Gomez:** Methodology, Formal analysis, Investigation. **Santiago Loya-López:** Methodology, Formal analysis, Investigation. **E.M. Kithsiri Wijeratne:** Methodology, Formal analysis, Investigation. **Harrison Stratton:** Methodology, Formal analysis, Investigation. **Cheng Tang:** Methodology, Formal analysis, Investigation. **Paz Duran:** Methodology, Formal analysis, Investigation. **Kyleigh Masterson:** Methodology, Formal analysis, Investigation. **Omar Alsbiei:** Methodology, Formal analysis, Investigation. **A.A. Leslie Gunatilaka:** Conceptualization, Writing – review & editing, Supervision, Project administration, Funding acquisition. **Rajesh Khanna:** Conceptualization, Writing – original draft, Writing – review & editing, Supervision, Project administration, Funding acquisition.

Declaration of Competing Interest

The authors declare the following financial interests/personal relationships which may be considered as potential competing interests: R. K. is the founder of Regulonix LLC, a company developing nonopioid drugs for chronic pain. In addition, R.K., has patents US10287334 (non-narcotic CRMP2 peptides targeting sodium channels for chronic pain) and US10441586 (SUMOylation inhibitors and uses thereof) issued to Regulonix LLC. The other authors declare no conflicts.

Data availability

Data will be made available on request.

Acknowledgements

We thank Shizhen Luo for performing the SNI behavior experiments.

Funding Sources

Supported by National Institutes of Health awards from the National Institute of Neurological Disorders and Stroke (NS098772 and NS120663 to RK).

Declaration of Data Availability

This Declaration acknowledges that this paper adheres to the principles for transparent reporting and scientific rigor of preclinical research and that all data supporting the results are presented in the manuscript.

Appendix A. Supplementary data

Supplementary data to this article can be found online at https://doi.org/10.1016/j.ynpai.2023.100116.

References

Alles S.R.A., Smith P.A. 2017. The anti-allodynic gabapentinoids: myths, paradoxes, and acute effects. Neuroscientist. 23(1):40-55. Epub 20160708. doi: 10.1177/1073858416628793. PubMed PMID: 27118808.

Bauer, C.S., Nieto-Rostro, M., Rahman, W., Tran-Van-Minh, A., Ferron, L., Douglas, L., et al., 2009. The increased trafficking of the calcium channel subunit alpha2delta-1 to presynaptic terminals in neuropathic pain is inhibited by the alpha2delta ligand pregabalin. J Neurosci. 29 (13), 4076–4088. https://doi.org/10.1523/JNEUROSCI.0356-09.2009. PubMed PMID: 19339603; PubMed Central PMCID: PMC6665374.

Bell, T.J., Thaler, C., Castiglioni, A.J., Helton, T.D., Lipscombe, D., 2004. Cell-specific alternative splicing increases calcium channel current density in the pain pathway. Neuron 41 (1), 127–138. https://doi.org/10.1016/s0896-6273(03)00801-8. PubMed PMID: 14715140.

Bellampalli, S.S., Ji, Y., Moutal, A., Cai, S., Wijeratne, E.M.K., Gandini, M.A., et al., 2019. Betulinic acid, derived from the desert lavender Hyptis emoryi, attenuates paclitaxel-, HIV-, and nerve injury-associated peripheral sensory neuropathy via block of N- and T-type calcium channels. Pain. 160 (1), 117–135. https://doi.org/10.1097/j.

pain.0000000000001385. PubMed PMID: 30169422; PubMed Central PMCID: PMC6309937.
Bourinet, E., Altier, C., Hildebrand, M.E., Trang, T., Salter, M.W., Zamponi, G.W., 2014. Calcium-permeable ion channels in pain signaling. Physiol. Rev. 94 (1), 81–140. https://doi.org/10.1152/physrev.00023.2013. PubMed PMID: 24382884.
Brennan, T.J., Vandermeulen, E.P., Gebhart, G.F., 1996. Characterization of a rat model of incisional pain. Pain 64 (3), 493–502. https://doi.org/10.1016/0304-3959(95)01441-1. PubMed PMID: 8783314.
Cai S., Bellampalli S.S., Yu J., Li W., Ji Y., Wijeratne E.M.K., et al. 2019. (-)-Hardwickiic acid and hautriwaic acid induce antinociception via blockade of tetrodotoxin-sensitive voltage-dependent sodium channels. ACS Chem. Neurosci. 10(3):1716-28. Epub 20181220. doi: 10.1021/acschemneuro.8b00617. PubMed PMID: 30525440.
Cai S., Gomez K., Moutal A., Khanna R. 2021. Targeting T-type/CaV3.2 channels for chronic pain. Transl. Res. 234:20-30. Epub 20210107. doi: 10.1016/j.trsl.2021.01.002. PubMed PMID: 33422652; PubMed Central PMCID: PMC8217081.
Cai, S., Shan, Z., Zhang, Z., Moutal, A., Khanna, R., 2019. Activity of T-type calcium channels is independent of CRMP2 in sensory neurons. Channels (Austin) 13 (1), 147–152. https://doi.org/10.1080/19336950.2019.1608129. PubMed PMID: 31025580; PubMed Central PMCID: PMC6527066.
Cai, S., Moutal, A., Yu, J., Chew, L.A., Isensee, J., Chawla, R., et al., 2021. Selective targeting of NaV1.7 via inhibition of the CRMP2-Ubc9 interaction reduces pain in rodents. Sci. Transl. Med. 13 (619), eabh1314. https://doi.org/10.1126/scitranslmed.abh1314. PubMed PMID: 34757807.
Calderon-Rivera, A., Loya-Lopez, S., Gomez, K., Khanna, R., 2022. Plant and fungi derived analgesic natural products targeting voltage-gated sodium and calcium channels. Channels (Austin) 16 (1), 198–215. https://doi.org/10.1080/19336950.2022.2103234. PubMed PMID: 36017978. PubMed Central PMCID: PMC9423853.
Chaplan, S.R., Bach, F.W., Pogrel, J.W., Chung, J.M., Yaksh, T.L., 1994. Quantitative assessment of tactile allodynia in the rat paw. J. Neurosci. Methods 53 (1), 55–63. https://doi.org/10.1016/0165-0270(94)90144-9. PubMed PMID: 7990513.
Choe W., Messinger R.B., Leach E., Eckle V.S., Obradovic A., Salajegheh R., et al. 2011. TTA-P2 is a potent and selective blocker of T-type calcium channels in rat sensory neurons and a novel antinociceptive agent. Mol. Pharmacol. 80(5):900-10. Epub 20110805. doi: 10.1124/mol.111.073205. PubMed PMID: 21821734; PubMed Central PMCID: PMC3198916.
Darbaky, Y., Evrard, B., Patrier, S., Falenta, J., Garcin, S., Tridon, A., et al., 2017. Oral probiotic treatment of Lactobacillus rhamnosus Lcr35((R)) prevents visceral hypersensitivity to a colonic inflammation and an acute psychological stress. J. Appl. Microbiol. 122 (1), 188–200. https://doi.org/10.1111/jam.13320. PubMed PMID: 27718511.
Decosterd, I., Woolf, C.J., 2000. Spared nerve injury: an animal model of persistent peripheral neuropathic pain. Pain 87 (2), 149–158. https://doi.org/10.1016/s0304-3959(00)00276-1. PubMed PMID: 10924808.
Dreyfus, F.M., Tscherter, A., Errington, A.C., Renger, J.J., Shin, H.S., Uebele, V.N., et al., 2010. Selective T-type calcium channel block in thalamic neurons reveals channel redundancy and physiological impact of I(T)window. J. Neurosci. 30 (1), 99–109. https://doi.org/10.1523/JNEUROSCI.4305-09.2010. PubMed PMID: 20053892; PubMed Central PMCID: PMC2880440.
DuBreuil D.M., Lopez Soto E.J., Daste S., Meir R., Li D., Wainger B., et al. 2021. Heat but not mechanical hypersensitivity depends on voltage-gated Ca(V)2.2 calcium channel activity in peripheral axon terminals innervating skin. J. Neurosci. 41(36):7546-60. doi: 10.1523/JNEUROSCI.0195-21.2021. PubMed PMID: 34353899; PubMed Central PMCID: PMC8425970.
Duran, P., Loya-Lopez, S., Ran, D., Tang, C., Calderon-Rivera, A., Gomez, K., et al., 2022. The natural product Argentatin C attenuates postoperative pain via inhibition of voltage-gated sodium and T-type voltage-gated calcium channels. Br. J. Pharmacol. https://doi.org/10.1111/bph.15974. PubMed PMID: 36245395.
Evans, A.R., Nicol, G.D., Vasko, M.R., 1996. Differential regulation of evoked peptide release by voltage-sensitive calcium channels in rat sensory neurons. Brain Res. 712 (2), 265–273. https://doi.org/10.1016/0006-8993(95)01447-0. PubMed PMID: 8814901.
Felix, R., Calderon-Rivera, A., Andrade, A., 2013. Regulation of high-voltage-activated Ca(2+) channel function, trafficking, and membrane stability by auxiliary subunits. Wiley Interdiscip. Rev. Membr. Transp. Signal. 2 (5), 207–220. https://doi.org/10.1002/wmts.93. PubMed PMID: 24949251; PubMed Central PMCID: PMC4059758.
François-Moutal, L., Wang, Y., Moutal, A., Cottier, K.E., Melemedjian, O.K., Yang, X., et al., 2015. A membrane-delimited N-myristoylated CRMP2 peptide aptamer inhibits CaV2.2 trafficking and reverses inflammatory and postoperative pain behaviors. Pain 156 (7), 1247–1264. https://doi.org/10.1097/j.pain.0000000000000147. PubMed PMID: 25782368; PubMed Central PMCID: PMC5766324.
Gadotti V.M., Caballero A.G., Berger N.D., Gladding C.M., Chen L., Pfeifer T.A., et al. 2015. Small organic molecule disruptors of Cav3.2 - USP5 interactions reverse inflammatory and neuropathic pain. Mol. Pain. 11:12. Epub 20150314. doi: 10.1186/s12990-015-0011-8. PubMed PMID: 25889575; PubMed Central PMCID: PMC4364099.
Gao S., Yao X., Yan N. 2021. Structure of human Cav2.2 channel blocked by the painkiller ziconotide. Nature. 596(7870):143-7. doi: 10.1038/s41586-021-03699-6. PubMed PMID: 34234349; PubMed Central PMCID: PMC8529174.
Garcia-Caballero, A., Gadotti, V.M., Stemkowski, P., Weiss, N., Souza, I.A., Hodgkinson, V., et al., 2014. The deubiquitinating enzyme USP5 modulates neuropathic and inflammatory pain by enhancing Cav3.2 channel activity. Neuron 83 (5), 1144–1158. https://doi.org/10.1016/j.neuron.2014.07.036. PubMed PMID: 25189210.
Gomez, K., Tang, C., Tan, B., Perez-Miller, S., Ran, D., Loya, S., et al., 2022. Stereospecific effects of benzimidazolonepiperidine compounds on T-type Ca(2+) channels and pain. ACS Chem. Neurosci. https://doi.org/10.1021/acschemneuro.2c00256. PubMed PMID: 35671441.
Gris, G., Portillo-Salido, E., Aubel, B., Darbaky, Y., Deseure, K., Vela, J.M., et al., 2016. The selective sigma-1 receptor antagonist E-52862 attenuates neuropathic pain of different aetiology in rats. Sci. Rep. 6, 24591. https://doi.org/10.1038/srep24591. PubMed PMID: 27087602; PubMed Central PMCID: PMC4834548.
Guidelli, R. 2022. A historical biophysical dogma vs. an understanding of the structure and function of voltage-gated tetrameric ion channels. A review. Biochim. Biophys. Acta Biomembr. 1864(12):184046. 10.1016/j.bbamem.2022.184046 PubMed PMID: 36096197.
Harding, E.K., Zamponi, G.W., 2022. Central and peripheral contributions of T-type calcium channels in pain. Mol. Brain 15 (1), 39. https://doi.org/10.1186/s13041-022-00923-w. PubMed PMID: 35501819; PubMed Central PMCID: PMC9063214.
Heinke, B., Balzer, E., Sandkühler, J., 2004. Pre- and postsynaptic contributions of voltage-dependent Ca2+ channels to nociceptive transmission in rat spinal lamina I neurons. Eur. J. Neurosci. 19 (1), 103–111. https://doi.org/10.1046/j.1460-9568.2003.03083.x. PubMed PMID: 14750968.
Heppenstall, P.A., Lewin, G.R., 2006. A role for T-type Ca2+ channels in mechanosensation. Cell Calcium 40 (2), 165–174. https://doi.org/10.1016/j.ceca.2006.04.021. PubMed PMID: 16777219.
Hoppa, M.B., Lana, B., Margas, W., Dolphin, A.C., Ryan, T.A., 2012. alpha2delta expression sets presynaptic calcium channel abundance and release probability. Nature 486 (7401), 122–125. https://doi.org/10.1038/nature11033. PubMed PMID: 22678293; PubMed Central PMCID: PMC3376018.
Hoppanova L., Lacinova L. 2022. Voltage-dependent CaV3.2 and CaV2.2 channels in nociceptive pathways. Pflugers Arch. 474(4):421-34. Epub 20220118. doi: 10.1007/s00424-022-02666-y. PubMed PMID: 35043234.
Jacus, M.O., Uebele, V.N., Renger, J.J., Todorovic, S.M., 2012. Presynaptic Cav3.2 channels regulate excitatory neurotransmission in nociceptive dorsal horn neurons. J. Neurosci. 32 (27), 9374–9382. https://doi.org/10.1523/JNEUROSCI.0068-12.2012. PubMed PMID: 22764245; PubMed Central PMCID: PMC3398424.
Jagodic, M.M., Pathirathna, S., Nelson, M.T., Mancuso, S., Joksovic, P.M., Rosenberg, E. R., et al., 2007. Cell-specific alterations of T-type calcium current in painful diabetic neuropathy enhance excitability of sensory neurons. J. Neurosci. 27 (12), 3305–3316. https://doi.org/10.1523/JNEUROSCI.4866-06.2007. PubMed PMID: 17376991; PubMed Central PMCID: PMC6672477.
Jiang Y.Q., Andrade A., Lipscombe D. 2013. Spinal morphine but not ziconotide or gabapentin analgesia is affected by alternative splicing of voltage-gated calcium channel CaV2.2 pre-mRNA. Mol. Pain. 9:67. doi: 10.1186/1744-8069-9-67. PubMed PMID: 24369063; PubMed Central PMCID: PMC3916075.
Joksimovic S.L., Joksimovic S.M., Tesic V., Garcia-Caballero A., Feseha S., Zamponi G. W., et al. 2018. Selective inhibition of CaV3.2 channels reverses hyperexcitability of peripheral nociceptors and alleviates postsurgical pain. Sci. Signal. 11(545). doi: 10.1126/scisignal.aao4425. PubMed PMID: 30154101; PubMed Central PMCID: PMC6193449.
Kerckhove, N., Pereira, B., Soriot-Thomas, S., Alchaar, H., Deleens, R., Hieng, V.S., et al., 2018. Efficacy and safety of a T-type calcium channel blocker in patients with neuropathic pain: A proof-of-concept, randomized, double-blind and controlled trial. Eur. J. Pain 22 (7), 1321–1330. https://doi.org/10.1002/ejp.1221. PubMed PMID: 29577519.
Lauzadis, J., Liu, H., Lu, Y., Rebecchi, M.J., Kaczocha, M., Puopolo, M., 2020. Contribution of T-type calcium channels to spinal cord injury-induced hyperexcitability of nociceptors. J. Neurosci. 40 (38), 7229–7240. https://doi.org/10.1523/JNEUROSCI.0517-20.2020. PubMed PMID: 32839232; PubMed Central PMCID: PMC7534916.
Lee, M., 2014. Z944: a first in class T-type calcium channel modulator for the treatment of pain. J. Peripher. Nerv. Syst. 19 (Suppl 2), S11–S12. https://doi.org/10.1111/jns.12080_2. PubMed PMID: 25269728.
Lipscombe, D., Lopez-Soto, E.J., 2021. Epigenetic control of ion channel expression and cell-specific splicing in nociceptors: Chronic pain mechanisms and potential therapeutic targets. Channels (Austin) 15 (1), 156–164. https://doi.org/10.1080/19336950.2020.1860383. PubMed PMID: 33323031; PubMed Central PMCID: PMC7808434.
Liu, Q.Y., Chen, W., Cui, S., Liao, F.F., Yi, M., Liu, F.Y., et al., 2019. Upregulation of Cav3.2 T-type calcium channels in adjacent intact L4 dorsal root ganglion neurons in neuropathic pain rats with L5 spinal nerve ligation. Neurosci. Res. 142, 30–37. https://doi.org/10.1016/j.neures.2018.04.002. PubMed PMID: 29684385.
Liu, Q., Chen, W., Fan, X., Wang, J., Fu, S., Cui, S., et al., 2019. Upregulation of interleukin-6 on Cav3.2 T-type calcium channels in dorsal root ganglion neurons contributes to neuropathic pain in rats with spinal nerve ligation. Exp. Neurol. 317, 226–243. https://doi.org/10.1016/j.expneurol.2019.03.005. PubMed PMID: 30872136.
McArthur, J.R., Motin, L., Gleeson, E.C., Spiller, S., Lewis, R.J., Duggan, P.J., et al., 2018. Inhibition of human N- and T-type calcium channels by an ortho-phenoxyanilide derivative, MONIRO-1. Br. J. Pharmacol. 175 (12), 2284–2295. https://doi.org/10.1111/bph.13910. PubMed PMID: 28608537; PubMed Central PMCID: PMC5980596.
Miljanich, G.P., 2004. Ziconotide: neuronal calcium channel blocker for treating severe chronic pain. Curr. Med. Chem. 11 (23), 3029–3040. https://doi.org/10.2174/0929867043363884. PubMed PMID: 15578997.
Murali, S.S., Napier, I.A., Mohammadi, S.A., Alewood, P.F., Lewis, R.J., Christie, M.J., 2015. High-voltage-activated calcium current subtypes in mouse DRG neurons adapt in a subpopulation-specific manner after nerve injury. J. Neurophysiol. 113 (5), 1511–1519. https://doi.org/10.1152/jn.00608.2014. PubMed PMID: 25505111.

Muralidharan, A., Sotocinal, S.G., Austin, J.S., Mogil, J.S., 2020. The influence of aging and duration of nerve injury on the antiallodynic efficacy of analgesics in laboratory mice. Pain Rep. 5 (3), e824. https://doi.org/10.1097/PR9.0000000000000824. PubMed PMID: 32903926; PubMed Central PMCID: PMC7447376.

Nelson, M.T., Joksovic, P.M., Perez-Reyes, E., Todorovic, S.M., 2005. The endogenous redox agent L-cysteine induces T-type Ca2+ channel-dependent sensitization of a novel subpopulation of rat peripheral nociceptors. J. Neurosci. 25 (38), 8766–8775. https://doi.org/10.1523/JNEUROSCI.2527-05.2005. PubMed PMID: 16177046; PubMed Central PMCID: PMC6725512.

Nelson, M.T., Todorovic, S.M., 2006. Is there a role for T-type calcium channels in peripheral and central pain sensitization? Mol. Neurobiol. 34 (3), 243–248. https://doi.org/10.1385/MN:34:3:243. PubMed PMID: 17308355.

Nieto-Rostro, M., Ramgoolam, K., Pratt, W.S., Kulik, A., Dolphin, A.C., 2018. Ablation of alpha2delta-1 inhibits cell-surface trafficking of endogenous N-type calcium channels in the pain pathway in vivo. Proc. Natl. Acad. Sci. U. S. A. 115 (51), E12043–E12052. https://doi.org/10.1073/pnas.1811212115. PubMed PMID: 30487217; PubMed Central PMCID: PMC6305000.

Patel, R., Dickenson, A.H., 2016. Mechanisms of the gabapentinoids and alpha 2 delta-1 calcium channel subunit in neuropathic pain. Pharmacol. Res. Perspect. 4 (2) https://doi.org/10.1002/prp2.205. PubMed PMID: 27069626; PubMed Central PMCID: PMC4804325 e00205.

Perez-Reyes, E., 2003. Molecular physiology of low-voltage-activated t-type calcium channels. Physiol. Rev. 83 (1), 117–161. https://doi.org/10.1152/physrev.00018.2002. PubMed PMID: 12506128.

Piekarz A.D., Due M.R., Khanna M., Wang B., Ripsch M.S., Wang R., et al. 2012. CRMP-2 peptide mediated decrease of high and low voltage-activated calcium channels, attenuation of nociceptor excitability, and anti-nociception in a model of AIDS therapy-induced painful peripheral neuropathy. Mol. Pain. 8:54. Epub 20120724. doi: 10.1186/1744-8069-8-54. PubMed PMID: 22828369; PubMed Central PMCID: PMC3502107.

Ramachandra, R., Hassan, B., McGrew, S.G., Dompor, J., Farrag, M., Ruiz-Velasco, V., et al., 2013. Identification of CaV channel types expressed in muscle afferent neurons. J. Neurophysiol. 110 (7), 1535–1543. https://doi.org/10.1152/jn.00069.2013. PubMed PMID: 23843437; PubMed Central PMCID: PMC4042423.

Rose, K.E., Lunardi, N., Boscolo, A., Dong, X., Erisir, A., Jevtovic-Todorovic, V., et al., 2013. Immunohistological demonstration of CaV3.2 T-type voltage-gated calcium channel expression in soma of dorsal root ganglion neurons and peripheral axons of rat and mouse. Neuroscience 250, 263–274. https://doi.org/10.1016/j.neuroscience.2013.07.005. PubMed PMID: 23867767; PubMed Central PMCID: PMC3796369.

Saegusa, H., Matsuda, Y., Tanabe, T., 2002. Effects of ablation of N- and R-type Ca(2+) channels on pain transmission. Neurosci. Res. 43 (1), 1–7. https://doi.org/10.1016/s0168-0102(02)00017-2. PubMed PMID: 12074836.

Sanna, M.D., Les, F., Lopez, V., Galeotti, N., 2019. Lavender (Lavandula angustifolia Mill.), essential oil alleviates neuropathic pain in mice with spared nerve injury. Front Pharmacol. 10, 472. https://doi.org/10.3389/fphar.2019.00472. PubMed PMID: 31143116; PubMed Central PMCID: PMC6521744.

Schmidtko A., Lötsch J., Freynhagen R., Geisslinger G. 2010. Ziconotide for treatment of severe chronic pain. Lancet. 375(9725):1569-77. Epub 20100421. doi: 10.1016/s0140-6736(10)60354-6. PubMed PMID: 20413151.

Schroeder, J.E., Fischbach, P.S., McCleskey, E.W., 1990. T-type calcium channels: heterogeneous expression in rat sensory neurons and selective modulation by phorbol esters. J Neurosci. 10 (3), 947–951. PubMed PMID: 2156966; PubMed Central PMCID: PMC6570135.

Scroggs, R.S., Fox, A.P., 1992. Calcium current variation between acutely isolated adult rat dorsal root ganglion neurons of different size. J Physiol. 445, 639–658. https://doi.org/10.1113/jphysiol.1992.sp018944. PubMed PMID: 1323671; PubMed Central PMCID: PMC1180002.

Shan Z., Cai S., Yu J., Zhang Z., Vallecillo T.G.M., Serafini M.J., et al. 2019. Reversal of peripheral neuropathic pain by the small-molecule natural product physalin F via block of CaV2.3 (R-Type) and CaV2.2 (N-Type) voltage-gated calcium channels. ACS Chem. Neurosci. 10(6):2939-55. Epub 20190418. doi: 10.1021/acschemneuro.9b00166. PubMed PMID: 30946560.

Shields, S.D., Cavanaugh, D.J., Lee, H., Anderson, D.J., Basbaum, A.I., 2010. Pain behavior in the formalin test persists after ablation of the great majority of C-fiber nociceptors. Pain. 151 (2), 422–429. https://doi.org/10.1016/j.pain.2010.08.001. PubMed PMID: 20832171; PubMed Central PMCID: PMC2955806.

Silos-Santiago, I., Hannig, G., Eutamene, H., Ustinova, E.E., Bernier, S.G., Ge, P., et al., 2013. Gastrointestinal pain: unraveling a novel endogenous pathway through uroguanylin/guanylate cyclase-C/cGMP activation. Pain 154 (9), 1820–1830. https://doi.org/10.1016/j.pain.2013.05.044. PubMed PMID: 23748116.

Tibbs, G.R., Posson, D.J., Goldstein, P.A., 2016. Voltage-gated ion channels in the PNS: novel therapies for neuropathic pain? Trends Pharmacol Sci. 37 (7), 522–542. https://doi.org/10.1016/j.tips.2016.05.002. PubMed PMID: 27233519.

Tjolsen, A., Berge, O.G., Hunskaar, S., Rosland, J.H., Hole, K., 1992. The formalin test: an evaluation of the method. Pain 51 (1), 5–17. https://doi.org/10.1016/0304-3959(92)90003-T. PubMed PMID: 1454405.

Todorovic, S.M., Jevtovic-Todorovic, V., 2011. T-type voltage-gated calcium channels as targets for the development of novel pain therapies. Br. J. Pharmacol. 163 (3), 484–495. https://doi.org/10.1111/j.1476-5381.2011.01256.x. PubMed PMID: 21306582; PubMed Central PMCID: PMC3101611.

Tytgat, J., Vereecke, J., Carmeliet, E., 1988. Differential effects of verapamil and flunarizine on cardiac L-type and T-type Ca channels. Naunyn Schmiedebergs Arch. Pharmacol. 337 (6), 690–692. https://doi.org/10.1007/BF00175798. PubMed PMID: 2851108.

Tytgat, J., Pauwels, P.J., Vereecke, J., Carmeliet, E., 1991. Flunarizine inhibits a high-threshold inactivating calcium channel (N-type) in isolated hippocampal neurons. Brain Res. 549 (1), 112–117. https://doi.org/10.1016/0006-8993(91)90606-v. PubMed PMID: 1654169.

Tytgat, J., Vereecke, J., Carmeliet, E., 1996. Mechanism of L- and T-type Ca2+ channel blockade by flunarizine in ventricular myocytes of the guinea-pig. Eur. J. Pharmacol. 296 (2), 189–197. https://doi.org/10.1016/0014-2999(95)00691-5. PubMed PMID: 8838456.

Vicario, N., Turnaturi, R., Spitale, F.M., Torrisi, F., Zappala, A., Gulino, R., et al., 2020. Intercellular communication and ion channels in neuropathic pain chronicization. Inflamm. Res. 69 (9), 841–850. https://doi.org/10.1007/s00011-020-01363-9. PubMed PMID: 32533221.

Wallace, M., Duan, R., Liu, W., Locke, C., Nothaft, W., 2016. A randomized, double-blind, placebo-controlled, crossover study of the T-type calcium channel blocker ABT-639 in an intradermal capsaicin experimental pain model in healthy adults. Pain Med. 17 (3), 551–560. https://doi.org/10.1093/pm/pnv068. PubMed PMID: 26814294.

Walters E.T., Crook R.J., Neely G.G., Price T.J., Smith E.S.J. 2022. Persistent nociceptor hyperactivity as a painful evolutionary adaptation. Trends Neurosci. doi: 10.1016/j.tins.2022.12.007.

Weiss N., Zamponi G.W. 2019. T-type calcium channels: From molecule to therapeutic opportunities. Int, J, Biochem, Cell Biol. 108:34-9. Epub 20190114. doi: 10.1016/j.biocel.2019.01.008. PubMed PMID: 30648620.

Weiss, N., Zamponi, G.W., De Waard, M., 2012. How do T-type calcium channels control low-threshold exocytosis? Commun. Integr. Biol. 5 (4), 377–380. https://doi.org/10.4161/cib.19997. PubMed PMID: 23060963; PubMed Central PMCID: PMC3460844.

Zamponi, G.W., 2016. Targeting voltage-gated calcium channels in neurological and psychiatric diseases. Nat. Rev. Drug Discov. 15 (1), 19–34. https://doi.org/10.1038/nrd.2015.5. PubMed PMID: 26542451.

Zamponi, G.W., 2017. A crash course in calcium channels. ACS Chem. Neurosci. 8 (12), 2583–2585. https://doi.org/10.1021/acschemneuro.7b00415. PubMed PMID: 29131938.

Zamponi, G.W., Striessnig, J., Koschak, A., Dolphin, A.C., 2015. The physiology, pathology, and pharmacology of voltage-gated calcium channels and their future therapeutic potential. Pharmacol. Rev. 67 (4), 821–870. https://doi.org/10.1124/pr.114.009654. PubMed PMID: 26362469; PubMed Central PMCID: PMC4630564.

Zelaya C.E., Dahlhamer J.M., Lucas J.W., Connor E.M. 2020. Chronic pain and high-impact chronic pain among U.S. adults, 2019. NCHS Data Brief. (390):1-8. PubMed PMID: 33151145.

Zhou, Y., Cai, S., Moutal, A., Yu, J., Gomez, K., Madura, C.L., et al., 2019. The natural flavonoid naringenin elicits analgesia through inhibition of NaV1.8 voltage-gated sodium channels. ACS Chem. Neurosci. 10 (12), 4834–4846. https://doi.org/10.1021/acschemneuro.9b00547. PubMed PMID: 31697467.

Zhou Y., Cai S., Gomez K., Wijeratne E.M.K., Ji Y., Bellampalli S.S., et al. 2020. 1-O-Acetylgeopyxin A, a derivative of a fungal metabolite, blocks tetrodotoxin-sensitive voltage-gated sodium, calcium channels and neuronal excitability which correlates with inhibition of neuropathic pain. Mol. Brain. 13(1):73. Epub 20200511. doi: 10.1186/s13041-020-00616-2. PubMed PMID: 32393368; PubMed Central PMCID: PMC7216607.

Ziegler, D., Duan, W.R., An, G., Thomas, J.W., Nothaft, W., 2015. A randomized double-blind, placebo-, and active-controlled study of T-type calcium channel blocker ABT-639 in patients with diabetic peripheral neuropathic pain. Pain 156 (10), 2013–2020. https://doi.org/10.1097/j.pain.0000000000000263. PubMed PMID: 26067585; PubMed Central PMCID: PMC4770341.